Eur. Phys. J. D **38**, 455–470 (2006)
DOI: 10.1140/epjd/e2006-00057-7

**THE EUROPEAN PHYSICAL JOURNAL D**

# Study of the nuclear fusion in a muonic d$\mu^3$He complex

V.M. Bystritsky[1,a], M. Filipowicz[2], V.V. Gerasimov[1], P.E. Knowles[3], F. Mulhauser[4], N.P. Popov[5], V.P. Volnykh[1], and J. Woźniak[5]

[1] Joint Institute for Nuclear Research, Dubna 141980, Russia
[2] University of Science and Technology, Fac. of Fuels and Energy, 30059 Cracow, Poland
[3] Department of Physics, University of Fribourg, 1700 Fribourg, Switzerland
[4] University of Illinois at Urbana–Champaign, Urbana, Illinois 61801, USA
[5] University of Science and Technology, Fac. Phys. Nucl. Techniques, 30059 Cracow, Poland

Received 18 July 2005 / Received in final form 10 October 2005
Published online 21 March 2006 – 

**Abstract.** An experimental study of the nuclear fusion reaction in the charge-asymmetrical $d\mu^3$He complex ($d\mu^3\mathrm{He} \to \alpha$ (3.5 MeV) + $p$ (14.64 MeV)) is presented. The 14.64 MeV protons were detected by three pairs of Si($dE - E$) telescopes placed around the cryogenic target filled with $D_2 + {}^3$He gas at 34 K. The 6.85 keV $\gamma$ rays emitted during the de-excitation of the $d\mu^3$He complex were detected by a germanium detector. The measurements were performed at two $D_2 + {}^3$He target densities, $\varphi = 0.0585$ and $\varphi = 0.168$ (relative to liquid hydrogen density) with an atomic concentration of $^3$He $c_{^3\mathrm{He}} = 0.0496$. The values of the effective rate of nuclear fusion in $d\mu^3$He were obtained for the first time: $\tilde{\lambda}_f = (4.5^{+2.6}_{-2.0}) \times 10^5$ s$^{-1}$($\varphi = 0.0585$); $\tilde{\lambda}_f = (6.9^{+3.6}_{-3.0}) \times 10^5$ s$^{-1}$($\varphi = 0.168$). The $J = 0$ nuclear fusion rate in $d\mu^3$He was derived: $\lambda_f^{J=0} = (9.7^{+5.7}_{-2.6}) \times 10^5$ s$^{-1}$ ($\varphi = 0.0585$); $\lambda_f^{J=0} = (12.4^{+6.5}_{-5.4}) \times 10^5$ s$^{-1}$ ($\varphi = 0.168$).

**PACS.** 34.70.+e Charge transfer – 36.10.Dr Positronium, muonium, muonic atoms and molecules – 39.10.+j Atomic and molecular beam sources and techniques – 82.30.Fi Ion-molecule, ion-ion, and charge-transfer reactions

## 1 Introduction

The formation of muonic molecules of hydrogen isotopes and their nuclear reactions have been the subject of many experimental and theoretical studies [1–8]. As for studies on the formation of charge-asymmetrical muonic molecules of the form $h\mu Z$ ($h = p, d, t$, and $Z$ are nuclei with charge $Z > 1$) and their respective nuclear fusion, the situation is slightly different. The impetus to study such systems was the theoretical prediction and experimental observation of the molecular mechanism for charge exchange (MMCE) for $p\mu$ atoms on He nuclei [9,10]. In essence, the mechanism is the following. By colliding with a He atom in a H–He mixture (H = $H_2, D_2, T_2$ and He = $^3$He, $^4$He), the muonic hydrogen atom forms a muonic molecular complex $h\mu$He ($h = p, d, t$) in the excited $2p\sigma$ state. In the case of a deuterium–helium mixture, the complex may then decay from this state (see Fig. 1) via one of three channels:

$$
\begin{aligned}
d\mu + \mathrm{He} \xrightarrow{\lambda_{d\mathrm{He}}} [(d\mu\mathrm{He})^* e^-]^+ \quad &+ e^- \\
\downarrow & \\
\xrightarrow{\lambda_\gamma} \qquad [(d\mu\mathrm{He})^+ e^-] &+ \gamma \qquad (1a)\\
\xrightarrow{\lambda_p} \qquad [(\mu\mathrm{He})^+_{1s} e^-] &+ d \qquad (1b)\\
\xrightarrow{\lambda_e} \qquad (\mu\mathrm{He})^+_{1s} &+ d + e^-. \qquad (1c)
\end{aligned}
$$

If He = $^3$He, fusion reactions may occur

$$
\begin{aligned}
d\mu^3\mathrm{He} \xrightarrow{\tilde{\lambda}_f} \alpha + \mu + \mathrm{p}\ (14.64\ \mathrm{MeV}) \qquad (2a)\\
\xrightarrow{\tilde{\lambda}_{f\Gamma}} \mu^5\mathrm{Li} + \gamma\ (16.4\ \mathrm{MeV}). \qquad (2b)
\end{aligned}
$$

Thus, the fusion proceeds by the formation of a $d\mu$ atom, which, through a collision with a $^3$He atom, forms the $d\mu^3$He molecular system. This molecule has two primary spin states, $J = 1$ and $J = 0$ [1]; formation is favoured

[a] e-mail: bystvm@nusun.jinr.ru

[1] $J$ denotes the total angular momentum of the three particles.

by the former, fusion the latter [11]. In equations (1a–1c), $\lambda_\gamma$ is the $(d\mu\mathrm{He})^*$ molecular decay channel for the 6.85 keV $\gamma$-ray emission, $\lambda_e$ for the Auger decay, and $\lambda_p$ for the break-up process. The $d\mu$He molecule is formed with a rate $\lambda_{d\mathrm{He}}$. The main fusion process, equation (2a), occurs with the rate $\tilde{\lambda}_f$, whereas the reaction (2b), with associated rate $\tilde{\lambda}_{f\Gamma}$, has a branching ratio on the order of $10^{-4}$ [12].

The interest in further study of charge-asymmetrical systems is motivated by the ability to characterize the strong interaction in the ultralow energy region. Secondly, the calculations of the Coulomb three-body interaction can be tested. More precisely, these studies may allow us to

- measure the main characteristics of the strong interaction in the region of astrophysical particle collision energies (∼keV) in the entrance channel. It should be mentioned that nuclear fusion reactions in charge-asymmetrical muonic molecules are characterized by the same energy range of interest to astrophysics [13]. The properties of the strong interactions such as charge symmetry, isotopic invariance, and the character of P- and T-invariance have been experimentally established mainly in the MeV region and are not guaranteed for keV energy interactions. At the same time, the comparison of fusion rates in muonic molecules of mirror $dt$ and $d^3$He reactions could throw light on strong-interaction symmetries for small energies;
- test the calculation algorithm for nuclear fusion reaction rates in $\mu$-molecular complexes as well as for partial decay rates for the asymmetrical complexes via various channels;
- solve some existing astrophysical problems. The study of fusion reactions between light nuclei is relevant to the nuclear reactions which occurred during primordial nucleosynthesis following the Big Bang, as well as those occurring in stars. The present understanding of nuclear abundances in the galaxy points to a deficiency of light nuclei (except $^4$He) compared with predictions based on the theory of thermonuclear reactions and existing modes. To explain this phenomenon, modified star models are usually proposed, which assume that during the extrapolation of nuclear cross-sections from accelerator energies to the astrophysical region no resonances or other anomalies occur. It cannot be excluded, however, that the nuclear cross-sections have a resonant character, which could lead to intensive burning of light elements in stars. Therefore the investigation of nuclear fusion in the astrophysical range of energies is very important.

By now the experimental discovery of MMCE has been confirmed in a number of experiments studying muon transfer from $h\mu$ to He isotopes. Formation rates of the charge-asymmetrical $d\mu$He, and $p\mu$He systems were measured [14–23] and calculated [24–32] with good accuracy, and partial decay rates of such complexes were found.

In the past five years there has been renewed interest in studying charge asymmetrical complexes and in particular fusion in the $d\mu^3$He system. In the $d\mu^3$He complex from states with orbital momenta $J = 0$ and $J = 1$, and the experimental upper limits of the effective fusion rate, $\tilde{\lambda}_f$, averaged over the populations of the fine-structure states of the $d\mu^3$He complex.

**Table 1.** Experimental and calculated nuclear fusion rates, in $\mathrm{s}^{-1}$, in the $d\mu^3$He complex. $\tilde{\lambda}_f$ is the effective fusion rate (2a), $\lambda_f^{J=0}$ and $\lambda_f^{J=1}$ are the rates of fusion (2a) in the $d\mu^3$He complex from the $J = 0$ and $J = 1$ states, respectively.

| | experiment | | | |
|---|---|---|---|---|
| Refs. | [33] | [34] | [35] | [36] |
| $\tilde{\lambda}_f$ | $\leq 7 \times 10^7$ | $\leq 1.6 \times 10^5$ | $\leq 6 \times 10^4$ | $\leq 5 \times 10^5$ |

| | theory | | | | | |
|---|---|---|---|---|---|---|
| Refs. | [26] | [37] | [38] | [39,40] | [41] | [42] |
| $\lambda_f^{J=0}$ | | $3 \times 10^8$ | $3.8 \times 10^6$ | $\sim 10^6$ | $10^{11}$ | $1.9 \times 10^5$ |
| $\lambda_f^{J=1}$ | $10^6$ | | | | | $6.5 \times 10^2$ |

The nuclear fusion process following $d\mu^3$He molecular formation can occur via the intermediate resonant compound state $^5\mathrm{Li}^*$, leading to an expected high fusion rate which results from the large $S$–factor for the $d^3$He reaction [43]. However, from the calculations presented in Table 1, the theoretical fusion rate predictions in this molecule show a wide spread in value from $\sim 10^5$ $\mathrm{s}^{-1}$ to $10^{11}$ $\mathrm{s}^{-1}$. A brief discussion of the calculated fusion rates presented in Table 1 is given in Appendix A.

The nuclear fusion rate in muonic molecules is usually calculated on the basis of Jackson's idea [44] which allows the factorization of nuclear and molecular coordinates. In this case the nuclear fusion rate $\lambda_f$ is given by

$$\lambda_f = \frac{S}{(\pi M Z_1 Z_2)} \left|\Psi_{sc}(0)\right|^2, \tag{3}$$

described by the astrophysical $S$–factor, the reduced mass of the system $M$, the nuclear charges $Z_1$ and $Z_2$, and the three–body system wave function $\Psi_{sc}(0)$ averaged over the muon degrees of freedom and taken at distances comparable with the size of the nuclei, i.e., for $r \to 0$ since the nuclear force is short ranged.

It should be mentioned that, strictly speaking, asymmetric muonic molecules ($Z_1 \neq Z_2$) do not form bound states but correspond to resonant states of the continuous spectrum. In this case an analogue of equation (3) is given in reference [38] as

$$\lambda_f = \frac{S}{(\pi M Z_1 Z_2)} \frac{1}{2l+1} \frac{M k_0}{4\pi} \Gamma \left|\Psi_{sc}(0)\right|^2, \tag{4}$$

where $l$ is the orbital quantum number of the resonant state, $k_0$ is the relative momentum corresponding to the resonant energy, $\Gamma$ is the width of the molecular state and $\Psi_{sc}(0)$ is the wave function for the scattering state at resonant energy. In the limit of a narrow resonance, when $\Gamma \to 0$, equations (3) and (4) coincide. However, one should take into account the asymptotic part of the wave function responsible for in–flight fusion, including the possible interference between the resonant and nonresonant channels.

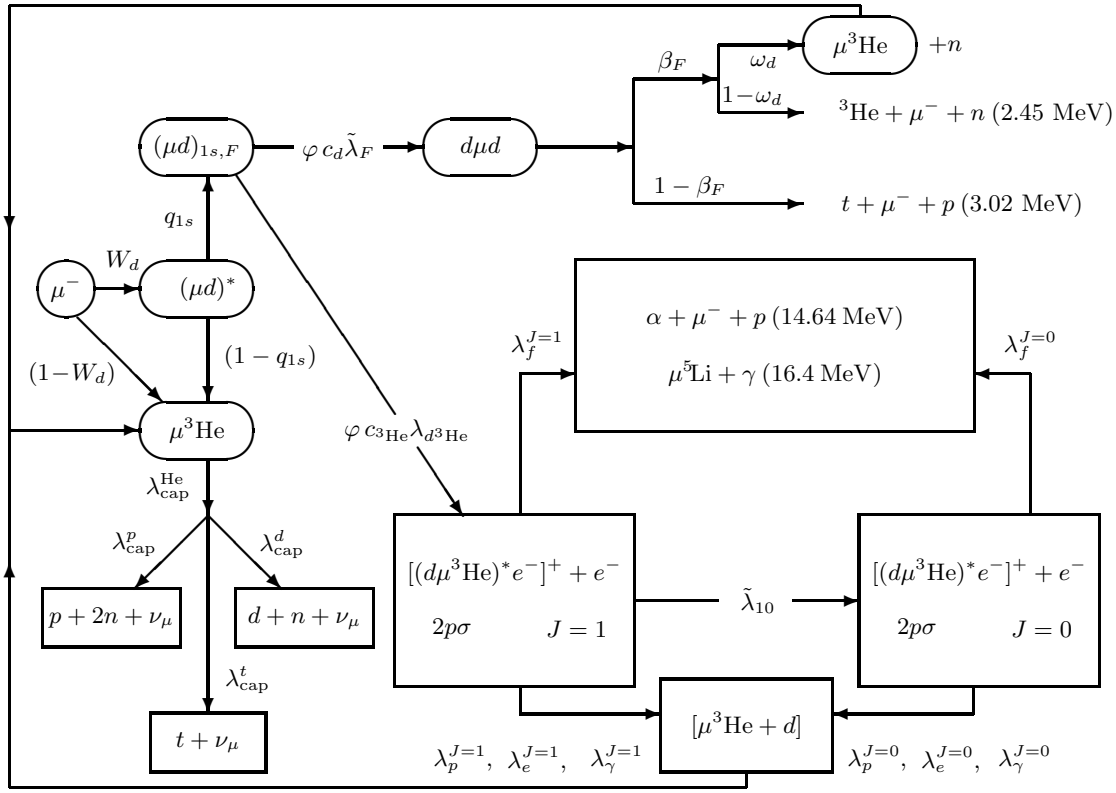


**Fig. 1.** Scheme of $\mu$-atomic and $\mu$-molecular processes when a negative muon is stopped in a $D_2 + {}^3$He mixture.

The different results of the fusion rate calculations in the $d\mu^3$He molecule reflect different approximations in the the solution to the Schrödinger equation for three particles with Coulomb interaction. The main uncertainty is associated with the results at small distances and hence generates the spread of the calculated fusion rate values given in Table 1. When the adiabatic expansion is used, the important problem of convergence of the expansion at small distances is usually ignored. Such problems vanish if the direct solution of the Fadeev equations in configuration space is performed [45–47]. For this reason the calculation of the fusion rate in the $d\mu^3$He molecule using Fadeev equations could be very important. The calculated results of this quantity (see Tab. 1) differ by several orders of magnitude.

Fewer studies were investigated the nuclear fusion reaction in $d\mu^3$He experimentally. An upper limit for the fusion reaction (2a) rate, has been found by a Gatchina–PSI collaboration using an ionization chamber [33–35]. Another experiment aimed at measuring the effective rate, $\tilde{\lambda}_{f,p}$, of reaction (2a) was performed by our team [36]. A preliminary result presenting an upper limit, is shown in Table 1.

The purpose of this work was to measure the effective rate, $\tilde{\lambda}_f$, of nuclear fusion reaction (2a) in the $d\mu^3$He complex via the production of a 14.64 MeV proton at two mixture densities.

## 2 Measurement method

Figure 1 shows a simplified version of the kinetics which occur when negative muons are stopped in the $D_2 + {}^3$He mixture. The information on the fusion reaction (2a) rate can be gained by measuring the time distribution, $dN_p/dt$, and the total yield, $N_p$, of 14.64 MeV protons. These quantities are derived from the differential equations governing the evolution of the $J = 1, 0$ states of the $d\mu^3$He molecules.

Establishing the time dependence of the number of $d\mu^3$He molecules, $N^J_{d\mu^3\mathrm{He}}(t)$, for the two possible states of $J$ is sufficient to predict the time spectrum of the fusion products. In the following, we will include the effective transition rate $\tilde{\lambda}_{10}$ of the $d\mu^3$He complex between the states $J = 1$ and $J = 0$. The $\tilde{\lambda}_{10}$ transition is important if the $\tilde{\lambda}^1_f$ and $\tilde{\lambda}^0_f$ rates differ greatly and an appropriate value of $\tilde{\lambda}_{10}$ permits the two rates to be measured. This possibility can be checked by measuring the fusion rate using different concentrations and densities which should also help clear up the questions surrounding the mechanism of the $\tilde{\lambda}_{10}$ transition [48], which is predicted to scale nonlinearly with the density.

There is a direct transfer from ground state $d\mu$'s to $^3$He's but that rate is about 200 times smaller than the $\lambda_{d^3\mathrm{He}}$ rate and will be ignored [49]. No hyperfine dependence on the $\lambda_{d^3\mathrm{He}}$ formation rate is expected since the

molecular formation involves an Auger electron and bound state energies of many tens of electron volts [9]. Muon recycling following $d\mu^3$He fusion is ignored due to the extremely small probability of the fusion itself, and thus the system of equations decouples into the $d\mu^3$He sector, and the $dd$–fusion sector (where cycling will be considered). Since there is no expectation of a $J = 0$ to $J = 1$ transition, i.e., $\lambda_{01}$, the $d\mu^3$He sector is easily solved.

The formation of $d\mu d$ molecules from a $d\mu$ in the hyperfine state $F = 3/2$ or $F = 1/2$ is given by the effective rate $\tilde{\lambda}_F$.

The probability, $W_d$, that the muon will be captured by a deuterium atom is

$$W_d = \frac{c_d}{c_d + Ac_{^3\mathrm{He}}} = \frac{X_{\mathrm{D}_2}}{X_{\mathrm{D}_2} + A' X_{^3\mathrm{He}}} \tag{5}$$

where $c_d$ and $c_{^3\mathrm{He}}$ are the deuterium and helium atomic concentrations. Here, $A$ is the relative muon atomic capture probability by a $^3$He atom compared to deuterium atom, and $A'$ is the same ratio measured with respect to gas fraction concentrations ($X$). The previous experimental measures for $\mathrm{D}_2 + {}^3$He give a mean value $A = 1.7 \pm 0.2$, cf. [16–18,50–52], and theoretical calculations for $A'$ have been made by Cohen [53]: for $\mathrm{D}_2 + {}^3$He: $A' = 0.78$ and for HD + $^3$He: $A' = 0.68$. Our gas mixtures have $c_{^3\mathrm{He}} = 0.0496(10)$ and thus $X_{^3\mathrm{He}} = 0.0946(20)$. From the atomic concentration, and using the experimental value, we get $W_d = 0.92(2)$. Using theory and the gas fraction the result is the same, $W_d = 0.92$.

The differential equations governing the evolution of the $J = 1, 0$ spin states of the $d\mu^3$He molecules are (see Fig. 1):

$$\frac{dN^1_{d\mu^3\mathrm{He}}}{dt} = +\varphi c_{^3\mathrm{He}} \lambda_{d^3\mathrm{He}} N_{d\mu} - \lambda^1_\Sigma N^1_{d\mu^3\mathrm{He}} \tag{6}$$

$$\frac{dN^0_{d\mu^3\mathrm{He}}}{dt} = +\tilde{\lambda}_{10} N^1_{d\mu^3\mathrm{He}} - \lambda^0_\Sigma N^0_{d\mu^3\mathrm{He}} \tag{7}$$

where $N_{d\mu}$ is the number of $d\mu$ atoms, and with definitions

$$\lambda^1_\Sigma = \left(\lambda_0 + \lambda_p^{J=1} + \lambda_\gamma^{J=1} + \lambda_e^{J=1} + \lambda_f^{J=1} + \tilde{\lambda}_{10}\right) \tag{8}$$

$$\lambda^0_\Sigma = \left(\lambda_0 + \lambda_p^{J=0} + \lambda_\gamma^{J=0} + \lambda_e^{J=0} + \lambda_f^{J=0}\right), \tag{9}$$

where $\lambda_0$ ($= 0.455 \times 10^6$ s$^{-1}$) is the free muon decay rate.

The proton yield between two given times $t_1$ and $t_2$ following muon arrival is:

$$\begin{aligned} Y_p(t_1, t_2) &= Y_p^1(t_1, t_2) + Y_p^0(t_1, t_2) \\ &= N_\mu^{\mathrm{D/He}} \frac{\tilde{\lambda}_f}{\lambda_\Sigma} \frac{\varphi c_{^3\mathrm{He}} \lambda_{d^3\mathrm{He}} W_d q_{1s} \varepsilon_Y \varepsilon_p}{\lambda_{d\mu}}, \end{aligned} \tag{10}$$

where $\varepsilon_p$ is the proton detection efficiency and the difference in time exponents is defined as the yield efficiency:

$$\varepsilon_Y = \left(e^{\lambda_{d\mu} t_1} - e^{\lambda_{d\mu} t_2}\right), \tag{11}$$

and $\lambda_{d\mu}$ is the $d\mu$ atom disappearance rate

$$\begin{aligned} \lambda_{d\mu} = \lambda_0 &+ \varphi c_{^3\mathrm{He}} \lambda_{d^3\mathrm{He}} \\ &+ \varphi c_d \tilde{\lambda}_F \left[1 - W_d q_{1s} (1 - \beta_F \omega_d)\right]. \end{aligned} \tag{12}$$

The branching ratio $\beta_F$ and sticking probability $\omega_d$ determine the number of muons lost from the cycle by sticking and $q_{1s}$ represents the probability for a $d\mu$ atom formed in an excited state to reach the ground state [18]. The effective fusion rate is defined as

$$\tilde{\lambda}_f = \left(\lambda_f^{J=1} \frac{\lambda^0_\Sigma}{\tilde{\lambda}_{10} + \lambda^0_\Sigma} + \lambda_f^{J=0} \frac{\tilde{\lambda}_{10}}{\tilde{\lambda}_{10} + \lambda^0_\Sigma}\right), \tag{13}$$

$$\lambda_\Sigma = \lambda^0_\Sigma \left(\frac{\tilde{\lambda}_{10} + \lambda^1_\Sigma}{\tilde{\lambda}_{10} + \lambda^0_\Sigma}\right). \tag{14}$$

In the above equations, $N_\mu^{\mathrm{D/He}}$ is the number of muons stopped in the $\mathrm{D}_2 + {}^3$He mixture and $\varphi$ is the mixture atomic density relative to liquid hydrogen density (LHD, $N_0 = 4.25 \times 10^{22}$ cm$^{-3}$).

When protons are detected in coincidence with muon decay electrons, here often called the del-$e$ criterion, the fusion rate from equation (10) takes the form

$$\tilde{\lambda}_f = \frac{Y_p(t_1, t_2) \lambda_{d\mu} \lambda_\Sigma}{N_\mu^{\mathrm{D/He}} W_d q_{1s} \varphi c_{^3\mathrm{He}} \lambda_{d^3\mathrm{He}} \varepsilon_p \varepsilon_e \varepsilon_t \varepsilon_Y}, \tag{15}$$

where $\varepsilon_e$ is the detection efficiency for muon decay electrons and $\varepsilon_t$, defined as

$$\varepsilon_t = e^{-\lambda_0 t_{ini}} - e^{-\lambda_0 t_{fin}}, \tag{16}$$

is the time cut efficiency depending on the interval during which muon decay electrons are accepted. Note that equations (10–15) are valid when the proton detection times are $t \gg 1/\lambda_\Sigma$. The values $\varepsilon_p$ and $\lambda_\Sigma$ are found through calculation. An important feature of the present experiment is that $\tilde{\lambda}_f$ is found by using the experimental values of $\lambda_{d\mu}$, $\varepsilon_e$, $W_d$, $\lambda_{d^3\mathrm{He}}$, and $q_{1s}$ which are specific to our experimental conditions. The information on these quantities corresponds to the conditions of a particular experiment and is extracted by the analysis of yields and time distributions of the 6.85 keV $\gamma$-rays from reaction (1a), prompt and delayed X–rays of $\mu^3$He atoms in the $\mathrm{D}_2 + {}^3$He mixture and muon decay electrons. The quantity $\lambda_{d^3\mathrm{He}}$ is determined from equation (12) where $\beta_F = 0.58$, $\omega_d = 0.122(3)$ are taken from reference [54]. The effective $dd$ fusion rate $\tilde{\lambda}_F = 0.05 \times 10^6$ s$^{-1}$ is taken from reference [55]. The rate $\lambda_{d\mu}$ is the slope of the time distribution of $\gamma$-ray from reaction (1a). The procedure for measuring $q_{1s}$, $\lambda_{d^3\mathrm{He}}$, $W_d$, $\varepsilon_e$, $A$ and $\lambda_\gamma$ (the partial probability for the radiative $d\mu^3$He complex decay channel) as well as our results are described in detail in our previous work [23,56].

## 3 Experimental set-up

The experiment was performed at the $\mu$E4 beam line of the Paul Scherrer Institute (Switzerland) with a muon

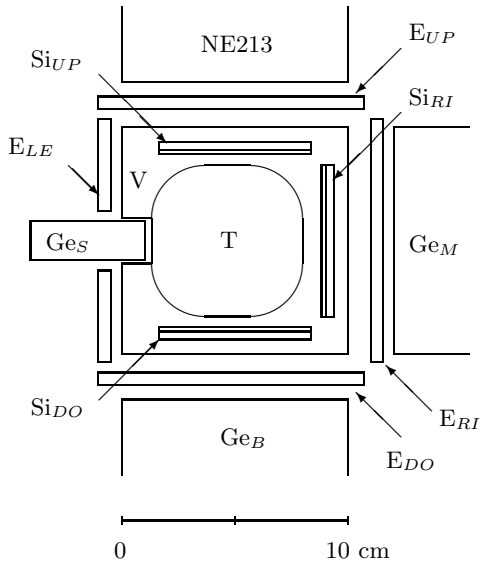


**Fig. 2.** Apparatus used in the $\mu$E4 area. The view is that of the incoming muon. The labels are explained in the text.

beam intensity near $2 \times 10^4$ s$^{-1}$. The experimental apparatus (see Fig. 2) was described in detail in references [23,56–59]. After passing through a thin plastic entrance counter muons entered the target and stopped there initiating the processes shown in Figure 1. The electronics rejected the arrival of two or more successive muons within a $\pm 10$ $\mu$s time window: this pileup rejection causes a 30% reduction in the effective muon beam. Thus, we have a number of "good muons", called $N_\mu$, stopping in our target.

Three pairs of Si($dE - E$) telescopes with a 42 mm diameter were installed directly behind 135 $\mu$m thick kapton windows to detect the 14.64 MeV protons from reaction (2a). They were made of a 4 mm thick Si($E$) detector and a thin, 360 $\mu$m thick, Si($dE$) detector, respectively. An assembly of Si detectors in this form gave a good identification of protons, deuterons, and electrons based on different energy losses of the above particles in those detectors. A 0.17 cm$^3$ germanium detector behind a 55 $\mu$m thick kapton window was used to detect the 6.85 keV $\gamma$-rays from reaction (1a). Muon decay electrons were detected by four pairs of scintillators, $E_{UP}$, $E_{DO}$, $E_{RI}$ and $E_{LE}$, placed around the vacuum housing of the target. The total solid angle of the electron detectors was ≈17%. To suppress muon decay electrons in the Si($dE - E$) telescope, provision was made in the electronic logic of the experiment to connect each of the electron detectors in anti-coincidence with the corresponding Si($dE - E$) telescope.

Our experiment included two runs with the $D_2 + {}^3$He mixture at different densities and with a helium atomic concentration of 5%. The experimental conditions are listed in Table 2. In addition, we performed different measurements with pure $D_2$, $^3$He, and $^4$He at different pressures and temperatures.

**Table 2.** Experimental conditions for the $D_2 + {}^3$He mixtures with an atomic concentration of helium $c_{^3\mathrm{He}} = 0.0496$. $N_\mu$ is the number of muons stopped in our apparatus.

| Run | $P_\mu$ [MeV/c] | $T$ [K] | $p$ [kPa] | $\varphi$ [LHD] | $N_\mu$ [$10^9$] |
|---|---|---|---|---|---|
| I | 34.0 | 32.8 | 513.0 | 0.0585 | 8.875 |
| II | 38.0 | 34.5 | 1224.4 | 0.1680 | 3.928 |

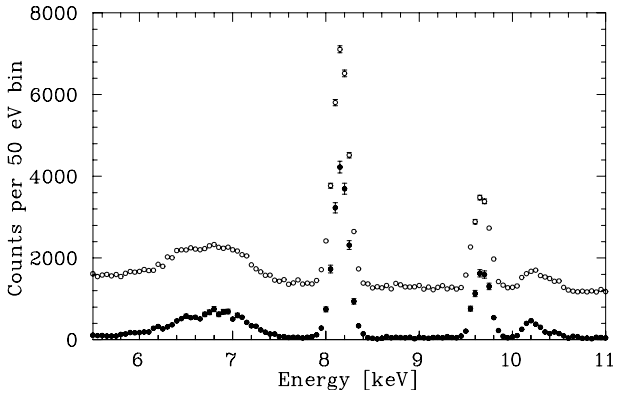


**Fig. 3.** Energy spectra of events detected by the $Ge_S$ detector in run I with (full circles) and without (open circles) the del-$e$ criterion.

The germanium detector was calibrated using $^{55}$Fe and $^{57}$Co sources. The Si($dE-E$) detectors were calibrated using a radioactive $^{222}$Rn source. Before the cryogenic target was assembled, a surface saturation of the Si($dE$) and Si($E$) detectors by radon was performed. The $^{222}$Rn decay with the emission of alpha-particles of energies 5.3, 5.5, 6.0, and 7.7 MeV were directly detected by each of the Si detectors. The linearity of the Si detector spectrometer electronics in the region of 8–15 MeV proton energy was checked using precision-amplitude pulse generators.

## 4 Analysis of the experimental data

### 4.1 Determination of the d$\mu^3$He complex formation rate

Figure 3 shows an example energy spectra of $\gamma$-ray events detected by the germanium detector in run I with and without the del-$e$ criterion. The rather wide peak on the left corresponds to the $\gamma$-rays with an average energy of 6.85 keV and the three right peaks correspond to the $K\alpha$, $K\beta$, $K\gamma$ lines of $\mu$He atoms with energies 8.17, 9.68, and 10.2 keV, respectively. As seen in Figure 3, the suppression factor for the background detected by the germanium detector with the del-$e$ criterion is of the order of $10^3$.

Figure 4 shows the time distribution of 6.85 keV $\gamma$-rays resulting from radiative de-excitation of the $d\mu^3$He complex in run I. The distribution was measured in coincidence with delayed muon decay electrons. The experimental time distribution of $\gamma$-rays shown in Figure 4 was

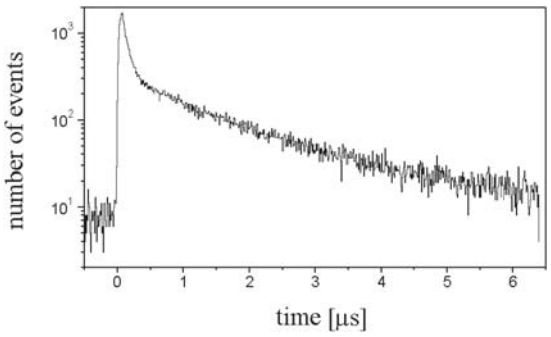


**Fig. 4.** Time distribution of the 6.85 keV $\gamma$–quanta resulting from radiative de-excitation of the $d\mu^3$He complex obtained in coincidence with a delayed muon decay electron from run I.

**Table 3.** Parameters measured from the $\gamma$-ray spectra used to determine the formation rates $\lambda_{d^3\mathrm{He}}$. The value $W_d = 0.92(2)$ was used for both runs.

| Run | $q_{1s}$ | $\lambda_{d\mu}$ [$10^6$ s$^{-1}$] | $\lambda_{d^3\mathrm{He}}$ [$10^6$ s$^{-1}$] |
|---|---|---|---|
| I | 0.882 (18) | $1.152(36)_{stat}(30)_{syst}$ | $240(13)_{stat}(15)_{syst}$ |
| II | 0.844 (20) | $2.496(58)_{stat}(100)_{syst}$ | $244(6)_{stat}(16)_{syst}$ |

approximated by the following expression

$$\frac{dN_\gamma}{dt} = B^\gamma e^{-\lambda_{d\mu}t} + C^\gamma e^{-\lambda_0 t} + D^\gamma, \qquad (17)$$

where $B^\gamma$, $C^\gamma$, and $D^\gamma$ are the normalization constants. The second and third terms in equation (17) describe the background contribution. The time analysis of the 6.85 keV $\gamma$-rays yielded values of $\lambda_{d\mu}$ and thus the formation rates $\lambda_{d^3\mathrm{He}}$ for the different density conditions. The results are given in Table 3.

The systematic error is larger than the uncertainty of the result caused by various possible background models (e.g., when the time structure of the background is inaccurately known), including the case where it is equal to zero. We have described the procedure for determining $\lambda_{d^3\mathrm{He}}$ in more detail in references [23,56].

### 4.2 Number of muon stops in the $D_2 + {}^3$He mixture

The number of muons stopped in the $D_2$+$^3$He mixture was determined by analyzing the time distributions of events detected by the four electron counters. We have discussed this matter in detail in references [23,56]. Below we recall some pertinent points in the determination of this value. To determine the number of muons stopped in the mixture, the time distribution of the detected electrons, $dN_e/dt$, is well approximated by an expression which is a superposition of four exponents and a background term $B^e$ from accidental events

$$\frac{dN_e}{dt} = A^e_{\mathrm{Al}} e^{-\lambda_{\mathrm{Al}}t} + A^e_{\mathrm{Au}} e^{-\lambda_{\mathrm{Au}}t} + A^e_{\mathrm{He}} e^{-\lambda_{\mathrm{He}}t} + A^e_{\mathrm{D}} e^{-\lambda_0 t} + B^e, \qquad (18)$$

where $A^e_{\mathrm{Al}}$, $A^e_{\mathrm{Au}}$, $A^e_{\mathrm{He}}$ and $A^e_{\mathrm{D}}$, are the normalized amplitudes with

$$A^e_i = N^i_\mu Q_i \lambda_0 \varepsilon_e \qquad i = \mathrm{Al},\ \mathrm{Au},\ \mathrm{He},\ \mathrm{D}, \qquad (19)$$

and

$$\lambda_{\mathrm{Al}} = Q_{\mathrm{Al}}\lambda_0 + \lambda^{\mathrm{Al}}_{\mathrm{cap}},$$
$$\lambda_{\mathrm{Au}} = Q_{\mathrm{Au}}\lambda_0 + \lambda^{\mathrm{Au}}_{\mathrm{cap}},$$
$$\lambda_{\mathrm{He}} = \lambda_0 + \lambda^{\mathrm{He}}_{\mathrm{cap}},$$

are the muon disappearance rates in the different elements found in the target (the rates are the inverse of the muon lifetimes in the target wall materials). The free muon decay and helium capture rates are $\lambda_0 = 0.455 \times 10^6$ s$^{-1}$ and $\lambda^{\mathrm{He}}_{cap} = 2216(70)$ s$^{-1}$ [61]. The nuclear capture rates in aluminum and gold, $\lambda^{\mathrm{Al}}_{\mathrm{cap}} = 0.7054(13) \times 10^6$ s$^{-1}$ and $\lambda^{\mathrm{Au}}_{\mathrm{cap}} = 13.07(28) \times 10^6$ s$^{-1}$, are taken from reference [60]. The Huff factors $Q_{\mathrm{Al}}$ and $Q_{\mathrm{Au}}$ take into account that muons are bound in the $1s$ state of the respective nuclei when they decay. This factor is negligible for helium but necessary for aluminum $Q_{\mathrm{Al}} = 0.993$ and important for gold $Q_{\mathrm{Au}} = 0.850$ [60].

We denote $N_\mu$ as the total number of muons stopped in the target, $N^{\mathrm{Al}}_\mu$, $N^{\mathrm{Au}}_\mu$, and $N^{\mathrm{D/He}}_\mu$ as the numbers of muons stopped in Al, Au, and the gaseous $D_2$ + $^3$He mixture, respectively. Thus, we have the relation

$$N_\mu = N^{\mathrm{Al}}_\mu + N^{\mathrm{Au}}_\mu + N^{\mathrm{D/He}}_\mu. \qquad (20)$$

Since muon decay via electron emission in the $D_2$ + $^3$He mixture takes place from the $1s$ state of the $d\mu$ or $\mu^3$He atom, the third and fourth terms in equation (18) will differ only by the amplitudes $A^e_{\mathrm{He}}$ and $A^e_{\mathrm{D}}$ because the slopes of both exponents are practically identical ($\lambda_{\mathrm{He}} = 0.457\mu\mathrm{s}^{-1}$, $\lambda_0 = 0.455\ \mu\mathrm{s}^{-1}$). Thus the following simplified expression was used to approximate the experimental electron time distributions

$$\frac{dN_e}{dt} = A^e_{\mathrm{Al}} e^{-\lambda_{\mathrm{Al}}t} + A^e_{\mathrm{Au}} e^{-\lambda_{\mathrm{Au}}t} + A^e_{\mathrm{D/He}} e^{-\tilde{\lambda}_{\mathrm{D/He}}t} + B^e. \qquad (21)$$

Under our experimental conditions of runs I and II, we obtained the effective rates $\tilde{\lambda}_{\mathrm{D/He}} = 0.4563\ \mu\mathrm{s}^{-1}$ and $0.4567\ \mu\mathrm{s}^{-1}$, respectively. With these effective muon decay rates, the difference between (18) and (21) is negligibly small. Figure 5 shows the time distribution of muon decay electrons measured in run I.

The amplitudes in equation (19) are expressed in terms of the factors $a_{\mathrm{Al}}$, $a_{\mathrm{Au}}$, and $a_{\mathrm{D/He}}$, defined as the partial muon stopping in Al, Au, and $D_2$ + $^3$He mixture,

$$a_i = \frac{N^i_\mu}{N_\mu}, \qquad \sum_i a_i = 1 \qquad i = \mathrm{Al},\ \mathrm{Au},\ \mathrm{D/He}; \qquad (22)$$

and take the new form

$$A^e_i = N_\mu \lambda_0 Q_i \varepsilon_e a_i. \qquad (23)$$

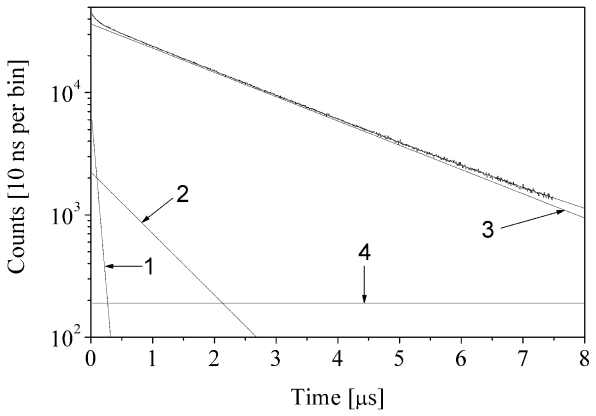


**Fig. 5.** Time distributions of muon decay electrons measured in run I. The solid curves are the results of fitting its components (see Eq. (21)): 1– Au; 2– Al; 3– $D_2 + {}^3$He; 4– constant background.

**Table 4.** Electron detection efficiencies, $\varepsilon_e$, in [%].

| Run | Detector | | | | |
|---|---|---|---|---|---|
| | $E_{UP}$ | $E_{RI}$ | $E_{DO}$ | $E_{LE}$ | all |
| I | 4.77(16) | 5.69(16) | 4.91(16) | 0.169(24) | 16.40(31) |
| II | 4.53(15) | 5.89(18) | 4.88(14) | 0.114(39) | 16.34(39) |
| $\varepsilon_e$ | 4.65(12) | 5.79(12) | 4.89(12) | 0.148(23) | 16.37(22) |

The electron detection efficiency, $\varepsilon_e$, of the detectors $E_{UP}$, $E_{DO}$, $E_{RI}$ and $E_{LE}$ was experimentally determined as a ratio between the number of events belonging to the $K$–lines of the $\mu^3$He atoms, found from the analysis of the data with and without the del-$e$ criterion,

$$\varepsilon_e = \frac{N_{x-e}}{N_x}, \tag{24}$$

where $N_{x-e}$ and $N_x$ are the numbers of events belonging to $K$–lines of the $\mu^3$He atom and detected by the germanium detector with and without coincidence with the electron detectors. Table 4 presents the results.

The electron detection efficiency of the detector $E_{LE}$ is considerably lower than that of each of the other three electron detectors. This is due to the thick layer of target material (Al, Fe) through which the muon decay electron had to pass to reach the $E_{LE}$ detector; the other electron detectors did not suffer from this unfavourable geometry.

Table 5 lists the muon stopping fractions in the $D_2 + {}^3$He mixture, $a_{D/He}$, found from the analysis of the time distributions of the events detected by the four electron detectors in runs I and II. The calculations of the $a_{D/He}$ fraction from equations (22) and (23) were performed with the assumption that the electron detection efficiency for each of the detectors $E_{UP}$, $E_{DO}$, $E_{RI}$ and $E_{LE}$ did not depend strongly on the coordinates of the muon stopping point in the target (be it in the target walls or in the $D_2 + {}^3$He mixture).

The systematic errors were fixed at one half of the maximum spread between the four $a_{D/He}$ values found from the individual time distribution analysis of the electrons detected by each of $E_{UP}$, $E_{DO}$, $E_{RI}$ and $E_{LE}$. Note that the fraction of muons stopped in gas, $a_{D/He}$, is a result of simultaneously fitting all time distributions obtained with each of the electron detectors (and not a result of averaging the results from the four detectors).

**Table 5.** Fraction, $a_{D/He}$, of muons stopped in the gaseous $D_2 + {}^3$He mixture. $N_\mu^{D/He}$ is the absolute number of muons stopped in the mixture.

| Run | $a_{D/He}$ | $N_\mu^{D/He}$ [$10^9$] |
|---|---|---|
| I | $0.475(6)_{stat}(30)_{syst}$ | 4.216 |
| II | $0.666(10)_{stat}(39)_{syst}$ | 2.616 |

### 4.3 Determination of the detection efficiency for 14.64 MeV protons

To determine the proton detection efficiency, $\varepsilon_p$, of the three Si($dE-E$) telescopes, one should know the distribution of muon stops over the target volume in runs I and II. The average muon beam momentum, $\overline{P}_\mu$, corresponding to the maximum fraction $a_{D/He}$ of muons stopped in the $D_2+{}^3$He mixture in runs I and II was found by varying $\overline{P}_\mu$ and analyzing the time distributions of the detected electrons using equation (21). For the given beam momentum and known beam momentum spread, we simulated the real distribution of muon stops in runs I and II by the Monte Carlo (MC) method [62]. The results of that simulation were used in another MC program to calculate the detection efficiency of each Si($dE-E$) detector pair for protons from reaction (2a). The MC algorithm [63] included simulation of the $d\mu$ and $\mu^3$He atom formation points and the entire chain of processes occurring in the mixture (cf. Fig. 1) from the instant when the muon hits the target to the decay or capture of the muon, or the possible production of 14.64 MeV protons in the fusion reaction in the $d\mu^3$He complex. The MC included the proton energy loss in the gas target, kapton windows, and in the thin Si($dE$) and thick Si($E$) detectors themselves. The proton detection efficiency $\varepsilon_p$ was calculated using the $q_{1s}$, $W_d$, and $\lambda_{d\mu}$ values (see Tab. 3) measured under our experimental conditions. The scattering cross-sections of $d\mu$ atoms for $D_2$ molecules were taken from references [64–66].

The simulation of the muon's evolution was halted when

(a) the muon either decays ($\mu^- \to e^-\nu_\mu\bar{\nu}_e$) or escapes the target;
(b) the muon is transferred from the deuteron to the $^3$He nucleus with the formation of a $^3$He$\mu$ atom;
(c) nuclear fusion occurs in the $d\mu^3$He complex;
(d) a $dd\mu \to p + t + \mu$ or $\to \mu^3\mathrm{He} + n$ occurs.

The MC also included the important background process of fusion–in–flight, which occurred from the following two

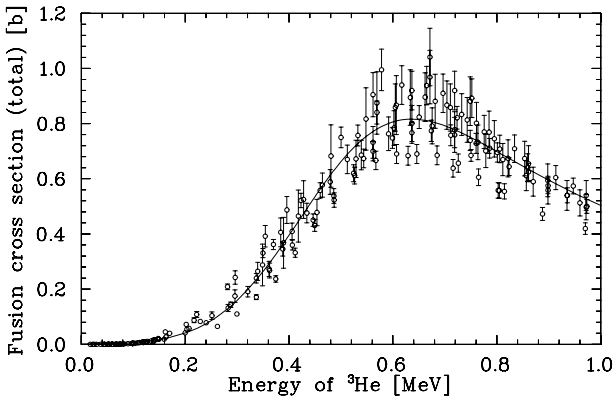


**Fig. 6.** Cross-section for the reaction $^3$He+$d \rightarrow {}^4$He+$p$ fusion–in–flight (reaction (25)) as a function of the $^3$He–deuteron collision energy. The solid curve is the result of averaging the entire set of the presented experimental data.

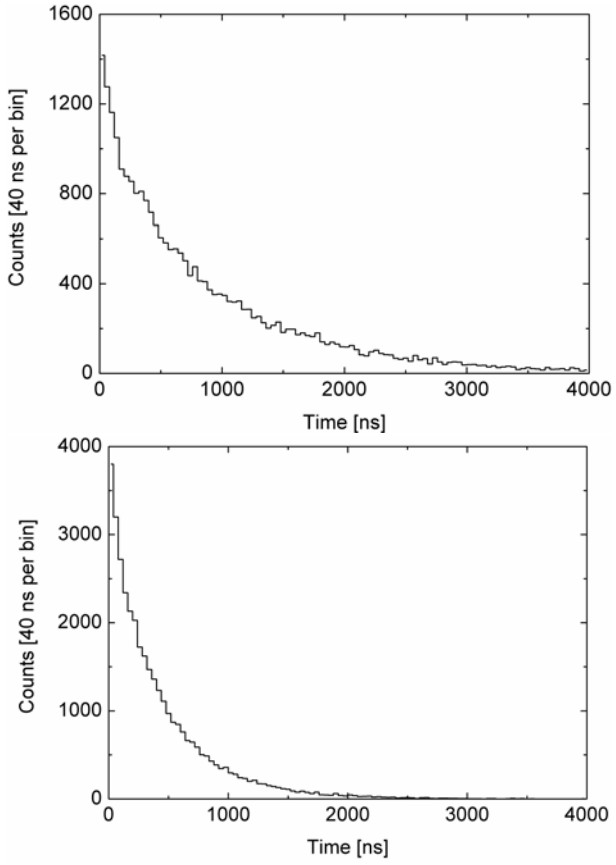


**Fig. 7.** MC calculated time distributions of the expected proton yield from reactions (2a) in runs I (left) and II (right).

reactions in succession:

$$d\mu + d \rightarrow dd\mu \rightarrow {}^3\mathrm{He}\,(0.8\ \mathrm{MeV}) + n \\ + \\ d \ \rightarrow \alpha + p(14.64\ \mathrm{MeV}). \quad (25)$$

In the calculations for reaction (25), we used the cross-section dependence on the $^3$He-deuteron collision energy averaged over the data from references [67–72] (Fig. 6).

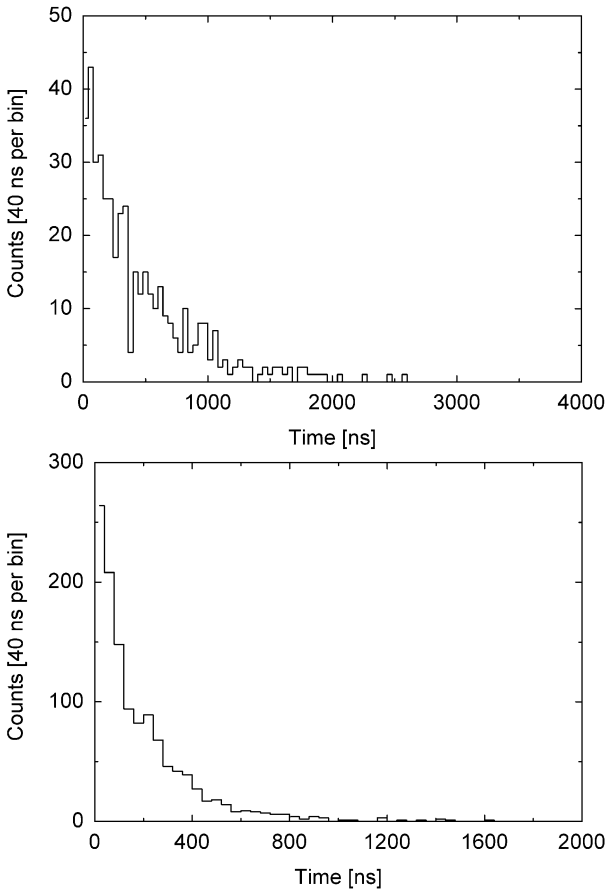


**Fig. 8.** MC calculated time distributions of the expected proton yield from background reactions (25) in runs I (left) and II (right).

The program also accounted for the energy loss of $^3$He nuclei in the $D_2 + {}^3$He mixture caused by ionization of $^3$He atoms and deuterium molecules. The accuracy of the simulation was analyzed by performing additional calculations with the input parameters (cross-sections, muon stops distributions, rates, etc.) varied within their uncertainties. The estimated error on the calculated detection efficiency for 14.64 MeV protons does not exceed 4%.

Under the same experimental conditions, the protons from reactions (2a) and (25) have completely different time distributions in accordance with the kinetics of the processes in the $D_2 + {}^3$He mixture. Figures 7 and 8 show the calculated time distributions of the expected proton yields from reactions (2a) and (25) under the conditions of runs I and II. Thus, there exists a time interval for events detected by the Si($dE - E$) detectors where the ratio of the yields from reaction (2a) and (25) is the largest. This, in turn, makes it possible to suppress the background detected from reaction (25) to a level low enough to meet the experimental requirement for the study of nuclear fusion in the $d\mu^3$He complex.

Calculated values for the quantities describing the muonic process kinetics in the $D_2$+$^3$He mixture and subsequent proton yield from reactions (2a) and (25) are shown in Table 6. The meaning of the quantities listed in this

**Table 6.** MC Calculated values of the quantities describing the muonic processes kinetics in the $D_2 + {}^3$He mixture (see text for explanation). The probabilities $W_{^3\mathrm{He}}$, $W_{d\mu^3\mathrm{He}}$, and $W_{d^3\mathrm{He}}$ are given per muon stopped in the mixture.

| Run | $W_{^3\mathrm{He}}$ $[10^{-2}]$ | $W_{d\mu^3\mathrm{He}}$ $[10^{-1}]$ | $W_{d^3\mathrm{He}}$ $[10^{-5}]$ | $W_{\mu e}$ $[10^{-1}]$ | $\varepsilon_p$ $[10^{-2}]$ | $\varepsilon_p^{ff}$ $[10^{-2}]$ | $\eta_p$ $[10^{-8}]$ | $\eta_p^{ff}$ $[10^{-8}]$ |
|---|---|---|---|---|---|---|---|---|
| I | 2.60 | 4.00 | 2.735 | 3.64 | 3.40 | 3.54 | 2.26 | 2.52 |
| II | 2.87 | 5.16 | 2.735 | 2.06 | 3.67 | 3.47 | 2.16 | 2.72 |

table is as follows: $W_{^3\mathrm{He}}$ is the total probability for energetic $^3$He production ($E_{^3\mathrm{He}} = 0.8$ MeV) in the $D_2 + {}^3$He mixture resulting from $dd\mu$ fusion; $W_{d\mu^3\mathrm{He}}$ is the $d\mu^3$He molecular formation probability; $W_{d^3\mathrm{He}}$ is the probability for $d^3$He fusion in flight, i.e., reaction (25); $W_{\mu e}$ is the muon decay branching ratio to the $\mu^- \to e^-\nu_\mu\bar{\nu}_e$ channel; $\varepsilon_p$ and $\varepsilon_p^{ff}$ are the detection efficiencies of one Si($dE-E$) telescope for protons from reactions (2a) and (25), respectively; $\eta_p$ and $\eta_p^{ff}$ are the proton yields from reactions (2a) and (25) detected by the Si($dE-E$) telescope per muon stopped in the gaseous $D_2 + {}^3$He mixture ($\lambda_f = 10^6$ s$^{-1}$ was used as the value for the $d\mu^3$He fusion rate for the calculation of $\eta_p$).

Figure 9 shows the two-dimensional event distributions detected by the Si($dE-E$) telescopes without coincidences with muon decay electrons in runs I and II. The vertical axis represents the energy losses in the thin Si($dE$) counter and the horizontal axis shows the total energy lost by the particle summed from both the Si($dE$) and Si($E$) detectors. The event distributions in Figure 9 corresponds to the detection of protons arising from both reactions (2a) and (25) and from capture background reactions such as

$$\begin{aligned} \mu + {}^3\mathrm{He} \quad &\to \quad p + 2n + \nu_\mu \\ \mu + \mathrm{Al} \to \mathrm{Na}^* \; &+p + n + \nu_\mu \\ &+p + \nu_\mu \\ &+p + 2n + \nu_\mu \\ \mu + \mathrm{Fe} \to \mathrm{Cr}^* \; &+p + n + \nu_\mu \\ &+p + \nu_\mu \\ &+p + 2n + \nu_\mu. \end{aligned} \tag{26}$$

In addition, the background which is not correlated with the muons stopped in the target (accidental coincidences) contributes to these distributions.

Figure 10 show the two-dimensional Si($dE-(E+dE)$) distributions obtained in coincidences with muon decay electrons. The use of the del-$e$ criterion leads to an appreciable reduction of the background (the suppression factor is ≈300 for the background), which in turn makes it possible to identify a rather weak effect against the intensive background signal.

The choice of the optimum criteria in the analysis of the Si($dE-E$) telescope data was reduced to the determination of the boundaries and widths of the time and energy intervals where the background was substantially suppressed in absolute value and the effect-to-background ratio was the best. To determine those intervals, the two-dimensional Si($dE-(dE+E)$) distributions corresponding to the detection of protons were simulated by MC for runs I and II. On the basis of those distributions, limits

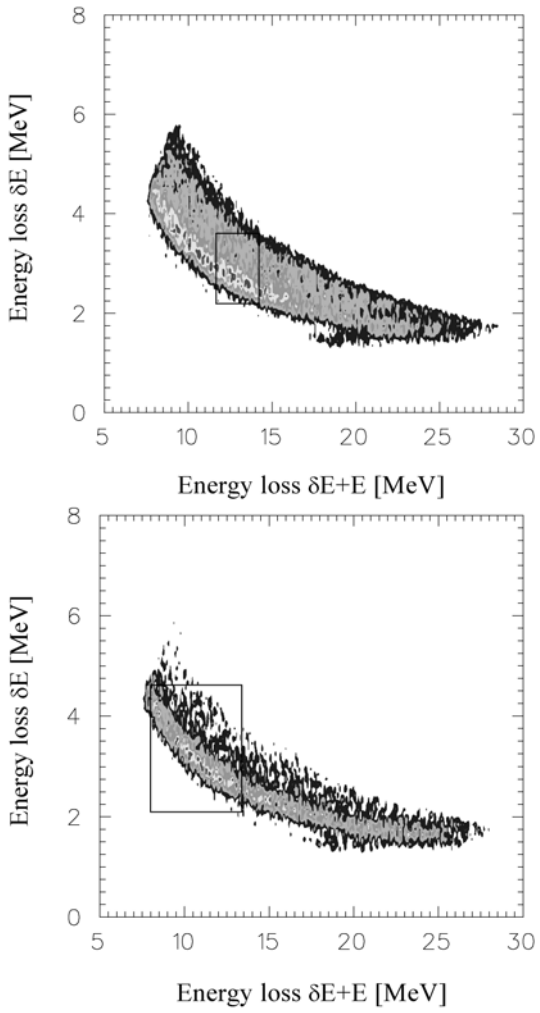


**Fig. 9.** Two-dimensional event distributions detected by the Si($dE-E$) telescopes in runs I (left) and II (right). The rectangles indicate the energy regions corresponding to the values of $\delta E$ and $\Delta E_\Sigma$ as found via MC.

were determined for the energy interval for protons from reaction (2a) where the loss of the "useful" event statistics collected by the Si telescope would be insignificant.

Figures 11 and 12 show the two-dimensional Si($dE-(dE+E)$) distributions corresponding to the proton detection which were simulated by the MC method for runs I and II. Based on these distributions, we chose some particular proton energy intervals called $\Delta E_\Sigma$ when considering the total energy deposited and called $\delta E$ when looking only at the Si($dE$) detector (see Tab. 7). Events from those intervals were used for further analysis. The event regions

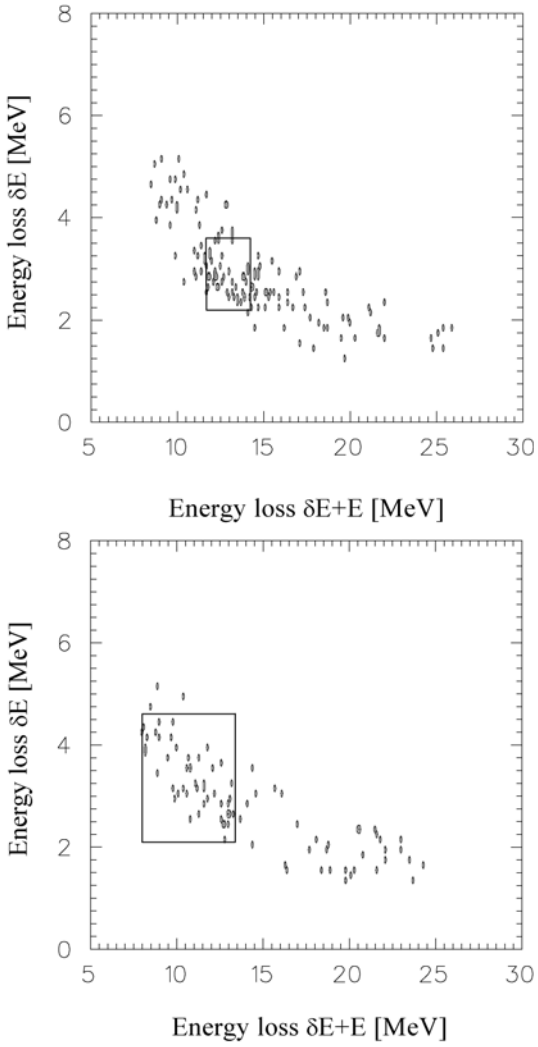


**Fig. 10.** Two-dimensional event distributions detected by the Si($dE-E$) telescopes in runs I (left) and II (right) with the del-$e$ coincidence. The rectangles indicate the energy regions corresponding to the chosen values of $\delta E$ and $\Delta E_\Sigma$ found by MC.

corresponding to the $\delta E$ and $\Delta E_\Sigma$ intervals are shown as rectangles on the two-dimensional distributions presented in Figures 9 and 10.

It is noteworthy that the proton detection efficiencies given in Table 6 correspond to these chosen proton energy intervals for runs I and II.

### 4.4 Analysis of the detected events

The next step in the data analysis was to choose particular time intervals for events detected by the Si($dE-E$) telescope. Table 7 presents the suppression factors of the statistics corresponding to the different initial time, $t_{thr}$, of the proton detection time interval and for the chosen proton energy intervals ($t_{thr}$ is taken with respect to the instant of the muon stop in the target). These factors correspond to the $\varepsilon_Y$ value in equation (10). The data in

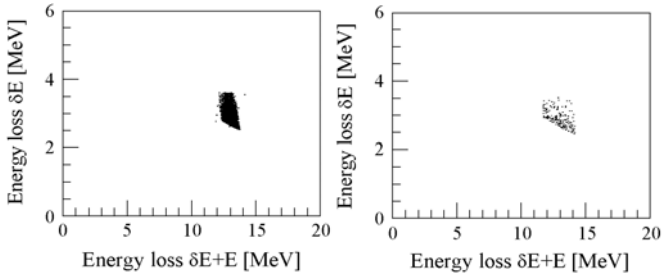


**Fig. 11.** Two-dimensional distributions of Si($dE-(dE+E)$) events obtained in run I by the Monte Carlo method and corresponding to the detection of protons from reactions (2a) (left) and (25) (right) within the time interval $\Delta t_{\rm Si}$.

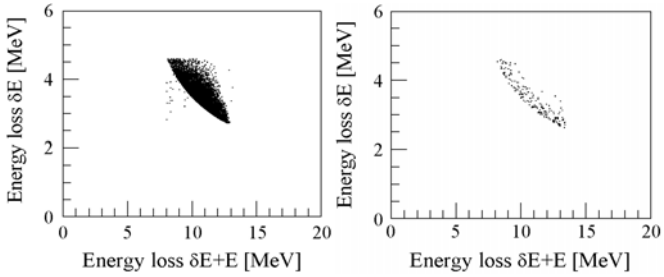


**Fig. 12.** Two-dimensional distributions of Si($dE-(dE+E)$) events obtained in run II by the Monte Carlo method and corresponding to the detection of protons from reactions (2a) (left) and (25) (right) within the time interval $\Delta t_{\rm Si}$.

Table 7 are derived from time distributions of the proton yields from reactions (2a) and (25) (see Figs. 7 and 8).

According to the data given in Table 7, we took the following time intervals $\Delta t_{\rm Si}$ (with $t_{\rm Si}$ the time of the Si signal) for analyzing the events

$$\begin{aligned} \Delta t_{\rm Si}\ \text{(run I)}: &\quad 0.7 \le t_{\rm Si} \le 2.2\ \mu\text{s} \\ \Delta t_{\rm Si}\ \text{(run II)}: &\quad 0.4 \le t_{\rm Si} \le 1.2\ \mu\text{s}. \end{aligned} \tag{27}$$

Figure 13 displays the two-dimensional distributions of Si($dE-E$) events obtained in coincidence with muon decay electrons in runs I and II with this time criteria imposed. With time intervals $\Delta t_{\rm Si}$ and the proton energy loss intervals $\Delta E_\Sigma$ and $\delta E$, the suppression factors of the statistics, $k_{d\mu^3{\rm He}}$, $k_{d^3{\rm He}}$, for events from reactions (2a) and (25) are, respectively,

$$\begin{aligned} k_{d\mu^3{\rm He}} &= 2.9 \qquad k_{d^3{\rm He}} = 11.2 \qquad \text{Run I} \\ k_{d\mu^3{\rm He}} &= 3.2 \qquad k_{d^3{\rm He}} = 12.1 \qquad \text{Run II}. \end{aligned} \tag{28}$$

The next stage of the data analysis was the determination of the number of events detected by the Si($dE-E$) telescopes in runs I and II under the following criteria:

(i) the coincidence of signals from the Si telescopes and electron detectors in the time interval $0.2 < (t_e - t_{\rm Si}) < 5.5$ $\mu$s ($t_e$ is the time of the electron detector signal with respect to muon arrival). Such a requirement adds the efficiency factor $\varepsilon_t = 0.83$ when determining the rates.

**Table 7.** Time factors for reaction (2a) and reaction (25) for the chosen energy intervals for protons detected by the Si($dE-E$) telescopes with detection beginning at time $t_{thr}$.

| Run | $\Delta E_\Sigma$ [MeV] | $\delta E$ [MeV] | Reaction (2a) $t_{thr}$, $\mu s^{-1}$ | | | | | Reaction (25) $t_{thr}$, $\mu s^{-1}$ | | | | |
|---|---|---|---|---|---|---|---|---|---|---|---|---|
| | | | 0.0 | 0.2 | 0.4 | 0.7 | 0.9 | 0.0 | 0.2 | 0.4 | 0.7 | 0.9 |
| I | $[0-\infty]$ | $[0-\infty]$ | 0.911 | 0.684 | 0.524 | 0.350 | 0.264 | 0.989 | 0.599 | 0.388 | 0.198 | 0.131 |
| | $[11.7-14.2]$ | $[2.1-3.6]$ | 0.878 | 0.659 | 0.505 | 0.337 | 0.254 | 0.438 | 0.263 | 0.171 | 0.090 | 0.058 |
| II | $[0-\infty]$ | $[0-\infty]$ | 0.934 | 0.543 | 0.316 | 0.129 | 0.059 | 0.996 | 0.333 | 0.114 | 0.025 | 0.009 |
| | $[8.0-13.4]$ | $[2.1-4.6]$ | 0.904 | 0.525 | 0.306 | 0.125 | 0.057 | 0.752 | 0.252 | 0.084 | 0.018 | 0.006 |

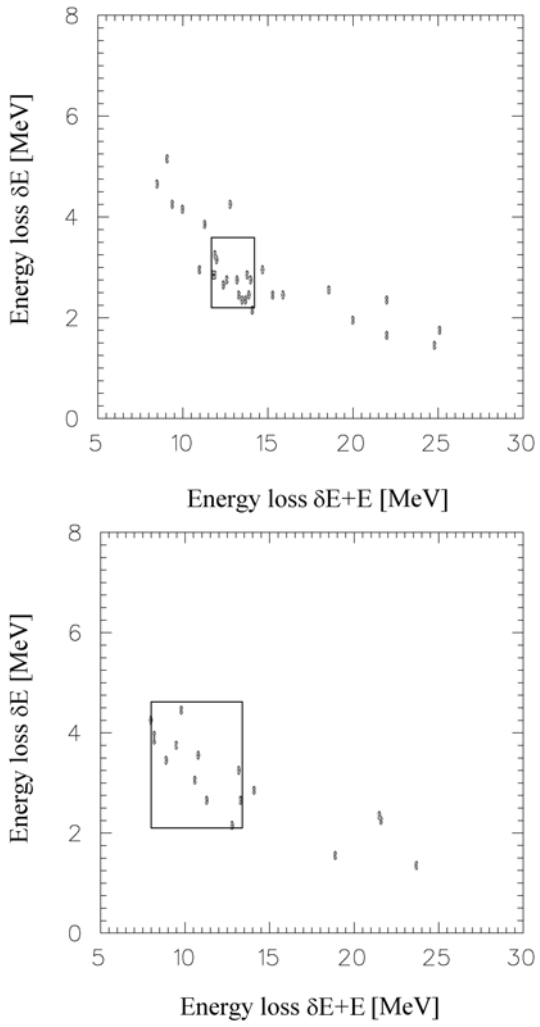


**Fig. 13.** Two-dimensional Si($dE-E$) telescope event distributions for runs I (left) and II (right) with the del-$e$ coincidence and the time interval $\Delta t_{\rm Si}$ as defined in equation (27).

(ii) the total energy release in the Si($dE$) detector is $\delta E$ as given in Table 7. For the thin and thick Si detector together, we choose the smallest interval, namely $\Delta E_\Sigma$ = [11.7−14.2] MeV for run I and $\Delta E_\Sigma$ = [8.0−13.4] MeV for run II.

The contribution of background events, $N_p^{ff}$, from reaction (25) is found in the following way. The expected number of detected protons from reaction (25) in runs I and II is calculated by

$$N_p^{ff} = \frac{N_\mu a_{\rm D/He} W_{^3\rm He} W_{d^3\rm He} \varepsilon_p^{ff} N_{\rm Si} \varepsilon_e \varepsilon_t}{k_{d^3\rm He}}, \qquad (29)$$

where $N_{\rm Si}$ is the number of Si($dE-E$) telescopes and $1/k_{d^3\rm He}$ is the background suppression factor generated by imposing criteria (i) and (ii) for the chosen time interval $\Delta t_{Si}$. Using the values of $a_{\rm D/He}$ and $N_\mu$ measured in runs I and II, the calculated values of $W_{^3\rm He}$, $W_{d^3\rm He}$, $\varepsilon_p^f$, $N_{\rm Si}$, $k_{d^3\rm He}$, $\varepsilon_t$, and equation (29), we obtained $N_p^{ff}$ (see Tab. 9). Errors of the calculated $N_p^{ff}$ arose from the inaccurate dependence of the cross-sections $\sigma_{d^3\rm He}$ for the $d^3$He reaction in flight on the $^3$He deuteron collision energy and from the errors in the calculation of the Si telescope detection efficiency for protons from reaction (25). These errors were found by substituting various experimental $\sigma_{d^3\rm He}(E_{d^3\rm He})$ dependencies [67–72] into the MC calculation of the in-flight $d^3$He fusion probability $W_{d^3\rm He}$.

**Table 8.** The three regions dividing the two-dimensional ($\delta E-\Delta E_\Sigma$) distributions as used for the background studies. All energies are given in MeV.

| | Region A | | Region B | | Region C | |
|---|---|---|---|---|---|---|
| Run | $\Delta E_\Sigma$ | $\delta E$ | $\Delta E_\Sigma$ | $\delta E$ | $\Delta E_\Sigma$ | $\delta E$ |
| I | 0–11.7 | 3.6–6 | 0–11.7 | 0–3.6 | 14.2–25 | 1.8–6 |
| II | 0–8 | 4.6–6 | 0–8 | 0–4.6 | 13.6–25 | 1.5–6 |

The level of the accidental coincidence background was found by analyzing the experimental data from runs I and II in the following way. The full two-dimensional distribution of events detected by the Si($dE-E$) telescopes was divided into three regions (A, B, and C), none of which included the region for events belonging to process (2a). The regions are given in Table 8.

The level of accidental coincidences of signals from the Si($dE-E$) telescopes and the electron detectors, $N_p^{acc}$, for the three given energy regions and the corresponding suppression factor of the accidental background in the Si telescopes, $\eta_{{\rm Si}-E}$, are defined as

$$N_p^{acc} = N_{\rm Si}^f \eta_{{\rm Si}-E}, \qquad (30)$$

$$\eta_{{\rm Si}-E} = \frac{\sum\limits_i N_{{\rm Si}-E}^i}{\sum\limits_i N_{\rm Si}^i}, \qquad (31)$$

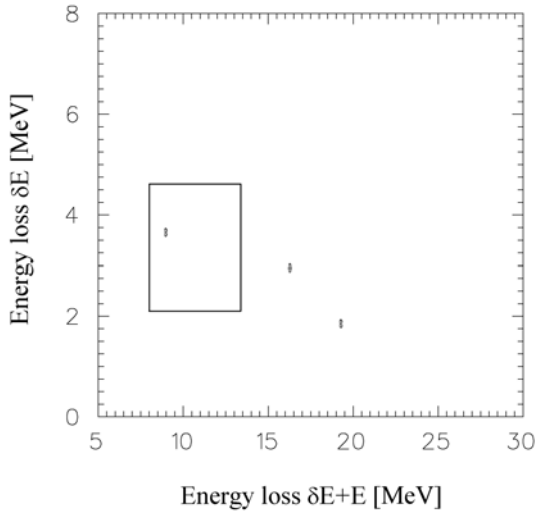


**Fig. 14.** Two-dimensional Si($dE-E$) telescope event distributions for a run with pure deuterium with the del-$e$ coincidences and within the $\Delta t_{\rm Si}$ interval. The rectangle is the region corresponding to the chosen energy intervals $\delta E$ and $\Delta E_\Sigma$ for detection events from reaction (2a) in the run with the $D_2 + {}^3$He mixture at $\varphi = 0.168$.

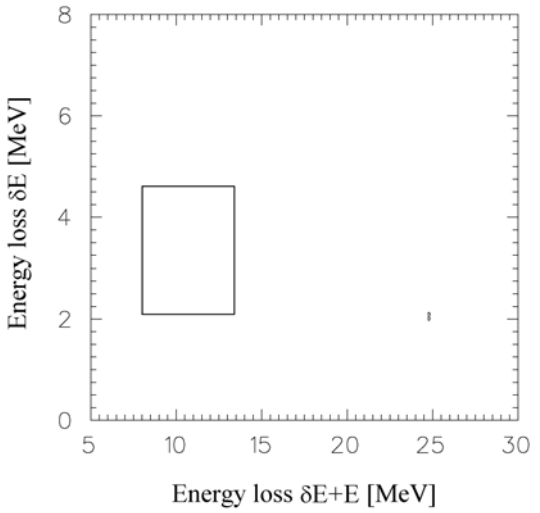


**Fig. 15.** Two-dimensional Si($dE-E$) telescope event distributions for a run with pure $^4$He with the del-$e$ coincidences and within the $\Delta t_{\rm Si}$ interval. The rectangle is the region corresponding to the chosen energy intervals $\delta E$ and $\Delta E_\Sigma$ for detection events from reaction (2a) in the run with the $D_2 + {}^3$He mixture at $\varphi = 0.168$.

where $N^f_{\rm Si}$ is the number of events detected by the three Si($dE-E$) telescopes belonging to the selected ($\delta E - \Delta E_\Sigma$) region for protons detected from reaction (2a). $N^i_{{\rm Si}-E}$ and $N^i_{\rm Si}$ are the number of detected events from the $i$th Si($dE-E$) telescope with and without del-$e$ coincidences and belonging to the A, B, and C regions. Note that the degree of accidental coincidence background suppression was determined not only by averaging the data obtained with the $D_2 + {}^3$He mixture but also by additional experiments with the targets filled with pure $^4$He, $D_2$, and $^3$He whose densities were: $^4$He — $\varphi \approx 0.11$ and $\varphi \approx 0.085$ ($N_\mu = 1.2 \times 10^9$); $D_2$ — $\varphi \approx 0.06 \div 0.17$ ($N_\mu = 1.5 \times 10^9$); $^3$He — $\varphi \approx 0.035$ ($N_\mu = 3.2 \times 10^9$). This guaranteed an identical ratio of stops in the target walls and in the gas for the experiments with $^4$He, $D_2$, $^3$He and the $D_2 + {}^3$He mixtures. Figures 14, 15, and 16 display the two-dimensional distributions of background events detected by the Si($dE-E$) telescopes in the experiments with $^4$He, $D_2$, and $^3$He.

The total numbers of detected background events, $N_p^{bckg}$, which belong to the analyzed energy region ($\delta E - \Delta E_\Sigma$) for protons from reaction (2a) and meeting the criteria (i)–(ii) were defined as

$$N_p^{bckg} = N_p^{ff} + N_p^{acc}. \quad (32)$$

Table 9 presents the number of detected events $N_p$, $N_p^{ff}$, $N_p^{acc}$, $N_p^{bckg}$ and $\eta_{Si-E}$ in runs I and II under the above criteria. The uncertainties of $N_p^{bckg}$ include both statistical and systematical errors.

Based on the measured $N_p$ and $N_p^{bckg}$ values we found the detected proton yield, $Y_p$, from reaction (2a) in runs I

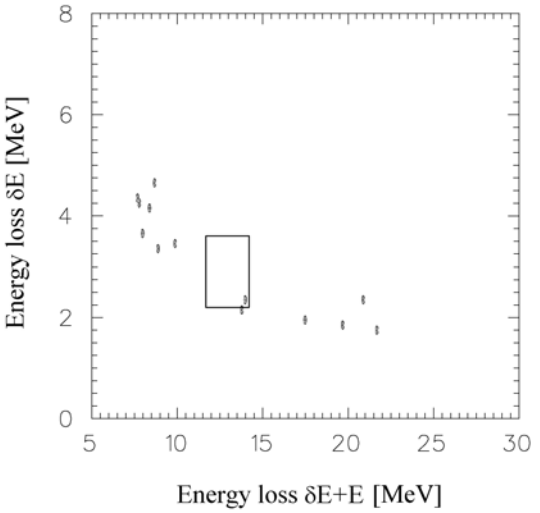


**Fig. 16.** Two-dimensional Si($dE-E$) telescope event distributions for a run with pure $^3$He with the del-$e$ coincidence and within the $\Delta t_{\rm Si}$ interval. The rectangle is the region corresponding to the chosen energy intervals $\delta E$ and $\Delta E_\Sigma$ for detection events from reaction (2a) in the run with the $D_2 + {}^3$He mixture at $\varphi = 0.0585$.

**Table 9.** Numbers of detected events, $N_p$ and $N_p^{ff}$ for the chosen $\delta E$ and $\Delta E_\Sigma$ intervals, taking into account the time intervals $t_e - t_{\rm Si}$, and $\Delta t_{\rm Si}$. The accidental coincidence background, $N_p^{acc}$, and the total background, $N_p^{bckg}$, are also shown.

| Run | $N_p$ | $N_p^{ff}$ | $\eta_{{\rm Si}-E}$ [$10^{-4}$] | $N_p^{acc}$ | $N_p^{bckg}$ |
|---|---|---|---|---|---|
| I | 14 | 3.8(2) | 4.2(8) | 2.5(5) | 6.3(6) |
| II | 11 | 2.4(1) | 2.4(11) | 1.1(5) | 3.5(5) |

**Table 10.** Effective rates of the $1 \to 0$ transition, $\tilde{\lambda}_{10}$, and the nuclear fusion rates in the $d\mu^3$He complex.

| Run | $\tilde{\lambda}_{10}$ $[10^{11}\ s^{-1}]$ | $\lambda_f^{J=0}$ $[10^5\ s^{-1}]$ | $\tilde{\lambda}_f$ $[10^5\ s^{-1}]$ | $\lambda_\Sigma$ $[10^{11}\ s^{-1}]$ |
|---|---|---|---|---|
| I | 5.2 | $9.7^{+5.7}_{-2.6}$ | $4.5^{+2.6}_{-2.0}$ | 6.54 |
| II | 7.5 | $12.4^{+6.5}_{-5.4}$ | $6.9^{+3.6}_{-3.0}$ | 6.44 |

and II:

$$Y_p = 7.7^{+4.4}_{-3.4} \qquad \text{run I}$$
$$Y_p = 7.5^{+3.8}_{-3.2} \qquad \text{run II.} \tag{33}$$

The errors of $Y_p$ are evaluated in accordance with references [73–75] dealing with analysis of small statistical samples.

To check the correctness of the choice of the energy region $[\delta E,\ \Delta E_\Sigma]$ selected for the analysis and presented in Table 7 additional calculations were performed. We varied the position of this energy window as well as its width and height up to 30% in different combinations and repeated the analysis of the experimental two-dimensional Si$(dE - E)$ telescope event distributions. The optimum $[\delta E,\ \Delta E_\Sigma]$ region was selected by the minimization of the $Y_p$ error.

### 4.5 Fusion rates. Discussion of the results

In view of equation (10) and the measured $Y_p$ values, the effective rate of nuclear fusion in the $d\mu^3$He complex is obtained from equation (15). It can be written as

$$\tilde{\lambda}_f = \frac{\lambda_{d\mu}\lambda_\Sigma}{N_\mu a_{\mathrm{D/He}} W_d q_{1s} \varphi c_{^3\mathrm{He}} \lambda_{d^3\mathrm{He}}} \frac{Y_p}{\varepsilon_p \varepsilon_e \varepsilon_t \varepsilon_Y}, \tag{34}$$

The values of $\tilde{\lambda}_f$ and $\lambda_\Sigma$ corresponding to the conditions of runs I and II are given in Table 10.

Using equation (13) with the measured effective nuclear fusion rate, assuming that $\lambda_f^1 \ll \lambda_f^0$ [42], one can find hypothetical estimates of the partial fusion rate in the $d\mu^3$He molecule in states with total orbital momentum $J = 0$ [2]

$$\lambda_f^{J=0} = \frac{\tilde{\lambda}_f(\tilde{\lambda}_{10} + \lambda_\Sigma^0)}{\tilde{\lambda}_{10}}. \tag{35}$$

The values for $\lambda_f^{J=0}$ found in runs I and II are also presented in Table 10.

The rates $\lambda_\Sigma^0 = 6 \times 10^{11}\ s^{-1}$ and $\lambda_\Sigma^1 = 7 \times 10^{11}\ s^{-1}$ (averaged from the data [26,27,30–32,39,76]) were used to extract the values presented in Table 10. The effective rate $\tilde{\lambda}_{10}$, for the transition of the $d\mu^3$He complex from the state with the angular momentum $J = 1$ to the state with $J = 0$, was calculated with allowance for the entire complicated branched chain of processes accompanying and competing with the rotational $1 \to 0$ transition. The chain of processes is considered in detail in references [11,77–79].

The effective rates of nuclear fusion in the $d\mu^3$He complex found by us in runs I and II coincide within the measurement errors. This is also true for the $d^3$He fusion rates $\lambda_f^{J=0}$ obtained by equation (35). A comparison of the measured $\lambda_f^{J=0}$ rate with the theoretical calculations show rather good agreement with [39], a slight discrepancy with references [38,42] and considerable disagreement with references [37,41]. The cause of this disagreement is not clear yet, nor is the discrepancy between $\lambda_f^{J=0}$ calculations in references [37–39,41] (see Tab. 1). Note that the theoretical papers (Refs. [37–39,41,42]) yield estimates with different degrees of approximation. A correct comparison of the experimental and theoretical $\lambda_f^{J=0}$ will be possible only after more experiments with the $D_2 + {}^3$He mixture with have eliminated the model dependence on the effective transition rate of the $d\mu^3$He complex from the $J = 1$ state to the $J = 0$ state.

A comparison of the results in this paper with the experimental results [35] reveals appreciable disagreement. The shortened form of result presentation in [35] does not allow us to discover the cause of this considerable disagreement. But as discussed in Appendix B, the upper limit of $\tilde{\lambda}_f$ is, in our mind, appreciably underestimated in the work of Maev et al. [35]. Another cause of the underestimation might be improper background subtraction procedures since they determined the background level using information from earlier experiments [34] carried out under different conditions at a different type of experimental facility. In addition, it is slightly surprising that the background from muon capture by $^3$He nuclei with the formation of protons in the energy region near 14.64 MeV is estimated at zero in reference [35][3].

We believe that our $\tilde{\lambda}_f$ measurement results are reliable, which is confirmed by the stable observation of nuclear fusion in both $D_2 + {}^3$He mixtures, which differed in density by a factor of about three. Nevertheless, as far as the experimental results obtained in this paper and in reference [35] are concerned, things are unfortunately uncertain and need clarifying.

There is an important point to consider when comparing the calculated rate $\lambda_f^{J=0}$ with the results of the previous experiment [35] and this paper. The measurement of $\lambda_f^{J=0}$ is indirect because it is determined by equation (35) with the calculated effective transition rate of the $d\mu^3$He molecule from the $J = 1$ to the $J = 0$ state. Therefore, $\lambda_f^{J=0}$ is not uniquely defined and greatly depends on $\tilde{\lambda}_{10}$,

[2] As follows from equation (35) $\lambda_f^{J=1}$ is absent there. It is explained by the quenching of the rate of the nuclear fusion reaction from $J = 1$ in comparison with $J = 0$, demonstrated in Table 1 (about three orders of magnitude). The strong interaction (i.e., fusion) is characterized by contact interaction of particles, realized at mutual distance $R \approx 0$. It is known that the maximum of s-wave function ($J = 0$) corresponds to $R = 0$, while the p-wave function ($J = 1$) is zero at the origin.

[3] According to reference [56], the fraction of protons from muon capture by the $^3$He nucleus in the energy range 14.3–14.64 MeV per $\mu^3$He atom is $W^p_{^3\mathrm{He}} = 2 \times 10^{-6}$.

which in turn is determined by the chain of processes accompanying and competing with the $1 \to 0$ transition.

For clarifying the above question it will be necessary to remove the ambiguity in the $\lambda_f^{J=0}$ determination and, in addition, to gain information on the effective $1 \to 0$ transition rate $\tilde{\lambda}_{10}$ and nuclear fusion rate $\lambda_f^{J=1}$ in the $J = 1$ state of $d\mu^3$He. This can be done, as proposed in references [77–79], in an experiment with the $D_2 + {}^3$He or $(H_2 + D_2(1\%) + {}^3$He) mixture with at least at three densities in the range $\varphi = 0.03$–$0.2$, where not only protons from reaction (2a) but also 6.85 keV $\gamma$ rays should be analyzed. We recommend also to increase by at least three times the detection efficiency for protons $\varepsilon_p$ and for muon decay electrons $\varepsilon_e$ in comparison with the present experiment in order to measure unambiguous and precise information on the important characteristics of $\mu$-molecular ($\lambda_{d\mu^3\mathrm{He}}$, $\tilde{\lambda}_{10}$) and nuclear ($\tilde{\lambda}_f$, $\lambda_f^{J=0}$, $\lambda_f^{J=1}$) processes occurring in the $D_2 + {}^3$He mixture.

The authors would like to thanks R. Jacot-Guillarmod for his help during the conception of this experiment. We are thankful to V.F. Boreiko, A. Del Rosso, O. Huot, V.N. Pavlov, V.G. Sandukovsky, V.A. Stolupin, F.M. Penkov, C. Petitjean, L.A. Schaller and H. Schneuwly for they help during the construction of the experiments, the data taking period, and for very useful discussions. This work was supported by the Russian Foundation for Basic Research, Grant No. 01–02–16483, the Polish State Committee for Scientific Research, the Swiss National Science Foundation, and the Paul Scherrer Institute.

## Appendix A

Let us briefly discuss the calculated nuclear fusion rates in the $d\mu^3$He reaction presented in Table 1. The values given in references [26,37] were given with some references to a calculation by Kamimura but without any references to the calculation method. In reference [38] the author used a small variation basis and the experimental value of the astrophysical factor $S \approx 6.32$ MeV $\times\, b$ and found the nuclear fusion rate in the $d\mu^3$He molecule in the $J = 0$ state to be $3.8 \times 10^6$ s$^{-1}$.

In references [39,40] the nuclear fusion rate in the $d\mu^3$He complex from the $J = 0$ state was calculated by various methods. Since the nuclear fusion rate in the $1s\sigma$ states of the $d\mu^3$He molecule is much higher than the fusion rate from the $2p\sigma$ state (because of a far smaller potential barrier), the under-barrier $2p\sigma \to 1s\sigma$ transition was calculated by finding the transition point in the complex $r$-plane. This procedure is not quite unambiguous and therefore the nuclear fusion rate in the $d\mu^3$He molecule was calculated in an alternative way by reducing it to the $S$–factor and using experimental data from low-energy scattering in ${}^3\mathrm{He}\,(dp)\,{}^4\mathrm{He}$ reactions from reference [39]. However, the approximation procedure of the experimental data for the ultralow energy region leads to some ambiguity in the results. The results of the calculation by the above two methods may differ by a factor of five for the $t\mu^3$He molecule and by a factor of three for the $d\mu^3$He molecule [40].

The highest nuclear fusion rate was obtained in reference [41]. Unlike the case in reference [40], where the barrier penetration factor in the $2p\sigma \to 1s\sigma$ transition was evaluated, reference [41] used the contribution from the $1s\sigma$ state to the total wave function for the small internuclear distances where $r$ was determined. The determination of the contribution from this state to the total mesomolecule wave function at small distance requires the solution of a multichannel system of differential equations; a complicated problem because of the singularity of the expansion coefficients at small distances $r \to 0$. As for the results of reference [42] given in the last column of Table 1, it is difficult to judge the calculation method used because the method for evaluating the wave function at small distances was not presented in the paper.

## Appendix B

Here are give reasons why some of the results of the intermediate calculations presented in reference [35] disagree with the real estimates of the calculated quantities.

(1) According to reference [35], the fraction of the $d\mu$ atoms which were formed in the excited state in their experimental conditions and arrived in the ground state (per muon stopped in the target) is $C_{d\mu} = 0.8$. The quantity $C_{d\mu}$ is defined as

$$C_{d\mu} = \frac{1}{2} W_{p,d} \left( q_{1s}^{p\mu} + q_{1s}^{d\mu} \right), \tag{B.1}$$

where $W_{p,d}$ is the probability for direct muon capture by the HD molecule followed by formation of the muonic hydrogen atom or the excited $d\mu$ atom. The q-factors, $q_{1s}^{p\mu}$ and $q_{1s}^{d\mu}$, are the probabilities for the transition of the $p\mu$ and $d\mu$ atoms from the excited state to the $1s$ ground state. According to references [21,56,80,81], for the Maev et al. experimental conditions the values of the quantities appearing in equation (B.1) were $W_{p,d} = 0.92$ $q_{1s}^{p\mu} = 0.5$, and $q_{1s}^{d\mu} = 0.8$. Thus, as follows from our estimation, $C_{d\mu} = 0.6$ and not 0.8 as stated.

(2) The number of $d\mu^3$He complexes formed over the duration of their experiment was defined as

$$N_{d\mu^3\mathrm{He}} = N_\mu C_{d\mu} \frac{\lambda_{d\mu^3\mathrm{He}}}{\lambda_{d\mu}}, \tag{B.2}$$

and correspond to $N_{d\mu^3\mathrm{He}} = (4.9 \pm 0.4) \times 10^8$. According to our estimates, the quantities $\lambda_{d\mu^3\mathrm{He}}$, $\lambda_{d\mu}$, $\lambda_{pd\mu}$ ($pd\mu$ molecule formation rate), and $N_{d\mu^3\mathrm{He}}$ had the values $\lambda_{d\mu^3\mathrm{He}} = 1.32 \times 10^6$ s$^{-1}$ ($\varphi = 0.0975$ $c_{^3\mathrm{He}} = 0.056$, $\lambda_{d^3\mathrm{He}} = 2.42 \times 10^8$ s$^{-1}$) [23],

$$\begin{aligned} \lambda_{d\mu} &\approx \lambda_0 + \lambda_{d\mu^3\mathrm{He}} \varphi c_{^3\mathrm{He}} + \lambda_{pd\mu} \varphi c_p + \tilde{\lambda}_F \omega_d \varphi c_d \\ &\approx 2.05 \times 10^6 \text{ s}^{-1}, \end{aligned}$$

$\lambda_{pd\mu} = 5.6 \times 10^6$ s$^{-1}$, which yields $N_{d\mu^3\mathrm{He}} \approx 3.7 \times 10^8$ s$^{-1}$ instead of $(4.9 \pm 0.4) \times 10^8$ s$^{-1}$.

(3) Their ionization chamber detection efficiency for protons from reaction (2a) was defined as $\varepsilon = \varepsilon_S \varepsilon_\tau$ and found to be $\varepsilon = 0.082$, where $\varepsilon_S = 0.13$ is the selection factor for events detected in compliance with certain amplitude and geometrical criteria, $\varepsilon_\tau = 0.63$ is the time factor to take into account that the detected events were analyzed in the time interval $0.4 \leq t \leq 1.8$ $\mu$s. According to our estimation, $\varepsilon_\tau = e^{-\lambda_{d\mu} t_1} - e^{-\lambda_{d\mu} t_2} = 0.44$, because under their experimental conditions the $d\mu$ disappearance rate is $\lambda_{d\mu} \approx 2.05 \times 10^6$ s$^{-1}$, $t_1 = 0.4$ $\mu$s, and $t_2 = 1.8$ $\mu$s.

## References


1. G.M. Marshall et al., Hyp. Interact. **138**, 203 (2001)
2. C. Petitjean, Hyp. Interact. **138**, 191 (2001)
3. C. Petitjean, Nucl. Phys. A **543**, 79c (1992)
4. J.S. Cohen, Muon Catal. Fusion **5/6**, 3 (1990/91)
5. L.I. Ponomarev, Contemp. Phys. **31**, 219 (1990)
6. L.I. Ponomarev, Hyp. Interact. **138**, 15 (2001)
7. K. Nagamine, Hyp. Interact. **138**, 5 (2001)
8. L.N. Bogdanova, V.E. Markushin, Nucl. Phys. A **508**, 29c (1990)
9. Y.A. Aristov et al., Yad. Fiz. **33**, 1066 (1981) [Sov. J. Nucl. Phys. **33**, 564 (1981)]
10. V.M. Bystritsky et al., Zh. Éksp. Teor. Fiz. **84**, 1257 (1983) [Sov. Phys. JETP **57**, 732 (1983)]
11. L.N. Bogdanova, S.S. Gershtein, L.I. Ponomarev, Pis'ma Zh. Éksp. Teor. Fiz. **67**, 89 (1998) [JETP Lett. **67**, 99 (1998)]
12. F.E. Cecil, D.M. Cole, R. Philbin, N. Jarmie, R.E. Brown, Phys. Rev. C **32**, 690 (1985)
13. J.L. Friar, B.F. Gibson, H.C. Jean, G.L. Payne, Phys. Rev. Lett. **66**, 1827 (1991)
14. D.V. Balin et al., Pis'ma Zh. Éksp. Teor. Fiz. **42**, 236 (1985) [JETP Lett. **42**, 296 (1985)]
15. H.P. von Arb et al., Muon Catal. Fusion **4**, 61 (1989)
16. V.M. Bystritsky et al., Kerntechnik **58**, 185 (1993)
17. V.M. Bystritsky, A.V. Kravtsov, N.P. Popov, Muon Catal. Fusion **5/6**, 487 (1990/91)
18. V.M. Bystritsky, A.V. Kravtsov, N.P. Popov, Zh. Éksp. Teor. Fiz. **97**, 73 (1990) [Sov. Phys. JETP **70**, 40 (1990)]
19. V.M. Bystritsky et al., Zh. Éksp. Teor. Fiz. **98**, 1514 (1990) [Sov. Phys. JETP **71**, 849 (1990)]
20. S. Tresch et al., Phys. Rev. A **57**, 2496 (1998)
21. B. Gartner et al., Phys. Rev. A **62**, 012501 (2000)
22. V.M. Bystritsky et al., Yad. Fiz. **58**, 808 (1995) [Phys. At. Nucl. **58**, 753 (1995)]
23. V.M. Bystritsky et al., Phys. Rev. A. **71**, 032723 (2005)
24. V.K. Ivanov et al., Zh. Éksp. Teor. Fiz. **91**, 358 (1986) [Sov. Phys. JETP **64**, 210 (1986)]
25. A.V. Kravtsov, A.I. Mikhailov, N.P. Popov, J. Phys. B **19**, 2579 (1986)
26. Y. Kino, M. Kamimura, Hyp. Interact. **82**, 195 (1993)
27. S.S. Gershtein, V.V. Gusev, Hyp. Interact. **82**, 185 (1993)
28. V.I. Korobov, V.S. Melezhik, L.I. Ponomarev, Hyp. Interact. **82**, 31 (1993)
29. W. Czapliński, A. Kravtsov, A. Mikhailov, N. Popov, Phys. Lett. A **233**, 405 (1997)
30. V.B. Belyaev, O.I. Kartavtsev, V.I. Kochkin, E.A. Kolganova, Phys. Rev. A **52**, 1765 (1995)
31. W. Czapliński, M. Filipowicz, E. Guła, A. Kravtsov, A. Mikhailov, N. Popov, Z. Phys. D **37**, 283 (1996)
32. V. Belyaev, O. Kartavtsev, V. Kochkin, E.A. Kolganova, Z. Phys. D **41**, 239 (1997)
33. D.V. Balin et al., Muon Catal. Fusion **7**, 301 (1992)
34. D.V. Balin et al., Gatchina Preprint 2221 NP–7 (1998)
35. E.M. Maev et al., Hyp. Interact. **118**, 171 (1999)
36. A. Del Rosso et al., Hyp. Interact. **118**, 177 (1999)
37. K. Nagamine et al., in *Muon–Catalyzed Fusion*, edited by S.E. Jones, J. Rafelski, H.J. Monkhorst (AIP Conference Proceedings 181, New York, 1989), p. 23 [Proceedings of the International Conference on Muon Catalyzed Fusion, $\mu$CF-88, Sanibel Island, USA, 1988]
38. F.M. Pen'kov, Yad. Fiz. **60**, 1003 (1997) [Phys. Atom. Nucl. **60**, 897 (1997)]
39. W. Czapliński, A. Kravtsov, A. Mikhailov, N. Popov, Phys. Lett. A **219**, 86 (1996)
40. W. Czapliński, A. Kravtsov, A. Mikhailov, N. Popov, Eur. Phys. J. D **3**, 223 (1998)
41. D. Harley, B. Müller, J. Rafelski, in *Muon–Catalyzed Fusion*, edited by S.E. Jones, J. Rafelski, H.J. Monkhorst (AIP Conference Proceedings 181, New York, 1989), pp. 239–244 [Proceedings of the International Conference on Muon Catalyzed Fusion, $\mu$CF-88, Sanibel Island, USA, 1988]
42. L.N. Bogdanova, V.I. Korobov, L.I. Ponomarev, Hyp. Interact. **118**, 183 (1999)
43. G.R. Gaughlan, W.A. Fowler, At. Data Nucl. Data Tables **40**, 283 (1988)
44. J.D. Jackson, Phys. Rev. **106**, 330 (1957)
45. A.A. Kostrykin, A.A. Kvitsinky, S.P. Merkuriev, Few–Body Systems **6**, 97 (1989)
46. C. Hu, A.A. Kvitsinsky, S.P. Merkuriev, Phys. Rev. A **45**, 2723 (1992)
47. C. Hu, A.A. Kvitsinsky, Phys. Rev. A **46**, 7301 (1992)
48. V.M. Bystritsky, W. Czapliński, N. Popov, Eur. Phys. J. D **5**, 185 (1999)
49. A.V. Matveenko, L.I. Ponomarev, Zh. Éksp. Teor. Fiz. **63**, 48 (1972) [Sov. Phys. JETP **36**, pp. 24–26 (1973)]
50. M. Bubak, V.M. Bystritsky, JINR Preprint E1–86–107, Dubna (1986)
51. V.M. Bystritsky et al., Nukleonika **40**, 51 (1995)
52. F. Kottmann, *Proc. Int. Symp. on Muon and Pion Interactions with Matter*, JINR, Dubna, D14-87-799 (1987) p. 268
53. J.S. Cohen, Phys. Rev. A **59**, 4300 (1999)
54. D.V. Balin et al., Pis'ma Zh. Éksp. Teor. Fiz. **40**, 318 (1984) [JETP Lett. **40**, 1112 (1984)]
55. C. Petitjean et al., Hyp. Interact. **101/102**, 1 (1996)
56. V.M. Bystritsky et al., Phys. Rev. A **69**, 012712 (2004)
57. V.F. Boreiko et al., Nucl. Instrum. Meth. A **416**, 221 (1998)
58. V.S. Stolupin et al., Hyp. Interact. **119**, 373 (1999)
59. V.M. Bystritsky et al., PSI proposal R-98-02, 1998
60. T. Suzuki, D.F. Measday, J.P. Koalsvig, Phys. Rev. C **35**, 2212 (1987)
61. E.M. Maev et al., Hyp. Interact. **101/102**, 423 (1996)
62. R. Jacot-Guillarmod, *Stopping Code*, University of Fribourg (1997) (unpublished)
63. J. Woźniak, V.M. Bystritsky, R. Jacot-Guillarmod, F. Mulhauser, Hyp. Interact. **101/102**, 573 (1996)
64. C. Chiccoli et al., Muon Catal. Fusion **7**, 87 (1992)

65. A. Adamczak et al., At. Data Nucl. Data Tables **62**, 255 (1996)
66. V.S. Melezhik, J. Woźniak, Muon Catal. Fusion **7**, 203 (1992)
67. R.M. White, R.W.D. Resler, G.M. Hale, Tech. Rep. IEAE-NDS-177, International Atomic Energy Agency (1997) (unpublished)
68. W.E. Kunz, Phys. Rev. **97**, 456 (1955)
69. A.P. Kljuchaiev et al., Tech. Rep. 109, URSS Academy of Science (1956) (unpublished)
70. J.C. Allred et al., Phys. Rev. **88**, 425 (1952)
71. H.V. Argo, R.F. Taschek, H.M. Agnew, A. Hemmendinger, W.T. Leland, Phys. Rev. **87**, 612 (1952)
72. G. Freier, H. Holmgren, Phys. Rev. **93**, 825 (1954)
73. O. Helene, Nucl. Instrum. Meth. A **228**, 120 (1984)
74. O. Helene, Nucl. Instrum. Meth. A **212**, 319 (1983)
75. G.J. Feldman, R.D. Cousins, Phys. Rev. D **57**, 3873 (1998)
76. W. Czapliński, M. Filipowicz, E. Guła, A. Kravtsov, A. Mikhailov, N. Popov, Z. Phys. D **41**, 165 (1997)
77. V.M. Bystritsky, F.M. Pen'kov, Yad. Fiz. **62**, 316 (1999) [Phys. At. Nucl. **62**, 281 (1999)]
78. V.M. Bystritsky, M. Filipowicz, F.M. Pen'kov, Nucl. Instrum. Meth. A **432**, 188 (1999)
79. V.M. Bystritsky, M. Filipowicz, F.M. Pen'kov, Hyp. Interact. **119**, 369 (1999)
80. S. Tresch et al., Phys. Rev. A **58**, 3528 (1998)
81. S. Tresch et al., Hyp. Interact. **119**, 109 (1999)